

Correlated Model For Wafer Warpage Prediction of Arbitrarily Patterned Films

Gregory T. Ostrowicki
Texas Instruments, Inc.
Dallas, TX USA
gtoostrowicki@ti.com

Siva P. Gurum
Texas Instruments, Inc.
Dallas, TX USA
sgurum@ti.com

Amit Nangia
Texas Instruments, Inc.
Dallas, TX USA
a-nangia1@ti.com

Abstract— Increasing power and efficiency requirements are driving a need for more metal content in the silicon back end. After being subjected to high temperature passivation processes, the film stress can increase significantly and lead to warped wafers. Warpage of various metalized wafers was characterized across a broad range of variables. In addition to metal film content and wafer dimensions as primary factors for the warpage, we find a strong dependence on the design of the artwork itself. A methodology was thus developed to predict wafer warpage of arbitrarily patterned films. A multi-scale finite-element-based modeling approach was used for converting a patterned composite film stack into an effective orthotropic film for efficient wafer-level stress and warpage analysis. A robust modeling correlation to the measured warpage was achieved across many variables, in terms of both warpage magnitude and shape.

Keywords—wafer warpage, thin films, metal artwork, finite element analysis

I. INTRODUCTION

Silicon wafers become warped during processing due the mismatch strains between the various film materials and layers built up within the active film stack. One of the driving mechanisms for the warpage is due to thick metal films, which after being subjected to high processing temperatures can develop significant tensile stress and lead to warped wafers. Great care is taken during manufacturing to ensure robust process capability for handling such warped wafers. However as increasing power and efficiency requirements are driving a need for more metal content in the silicon back end, the impact on the wafer warpage needs to be comprehended.

An extensive corner study utilizing test chip wafers was performed to characterize the wafer warpage across a range of variables, including: different layout geometries, metal density, film thicknesses, wafer size, and pre/post backgrind wafer thickness. The complex warpage behavior observed, and the apparent dependencies on layout design, prompted development of a model to better understand the physics and improve predictability of the warpage. A multi-scale finite-element-based modeling approach was presented previously for converting a patterned composite film stack into an effective orthotropic film for efficient wafer-level stress and warpage analysis [1]. This work discusses further optimization

of this model, applying the model to the evaluated wafer conditions, and finally a robust correlation to the extensive empirical measurements.

II. THEORY

Starting with Stoney's formula, the curvature of a plate can be related to the film stress by

$$\sigma_f = \frac{h_s^2 E_s}{6R h_f (1 - \nu_s)} \quad (1)$$

where σ is the stress, R is the radius of curvature, E is the Young's modulus, h is the thickness, ν is the Poisson's ratio, and the subscripts f and s correspond to the film and substrate, respectively [1]. However the applicability of this formula is limited to the case where the substrate and film materials are isotropic linear elastic, the film is much thinner than the substrate, and the radius of curvature is much greater than the substrate thickness (i.e. $h_f \ll h_s \ll R$). It is also convenient to quantify the warpage of silicon wafers in terms of the warp, which for the case of uniform spherical warpage can be derived from simple geometry as

$$w \approx d^2/8R \quad (2)$$

where w is the warp, and d is the wafer diameter.

In practice (1) and (2) are only first-order accurate due to non-uniform stress and warpage, nonlinear geometric effects as the as warp magnitude increases [3], surface contact with fixtures, and gravity. These additional effects become even more pronounced for 300 mm wafers. Thus numerical models were developed for more sophisticated mechanical analysis of the stress and warpage.

III. EXPERIMENTS

A. Test Vehicles

A broad range of test chip designs with different topmost metal artwork was defined and used to fabricate a suite of patterned wafers for warpage characterization. The layouts spanned a range of top-metal area coverage from 37% to 72%,

as well as a diverse set of line widths and pattern arrangements. Top-metal films were deposited and patterned using a standard metallization process onto bare silicon oxide wafers. A polymer overcoat was then applied and cured at high temperature to increase the metal stress and resulting warpage. The DOE matrix also included two different metallization thicknesses of 9 μm and 13 μm , blanket and patterned polymer overcoat, and 300 mm diameter wafers. In addition, a separate set of wafers was processed through backgrind to characterize the warpage after wafer thinning to ~ 10 and ~ 7 mils.

B. Warpage Measurement Methodology

Wafer warpage was characterized using an optical 3D contour scanner with demonstrated $\pm 30 \mu\text{m}$ accuracy. Here the wafers were placed on a flat surface with the patterned films facing upward. In this configuration the wafers were warped concave-up. The scanner then measured the standoff height at discrete points spanning laterally across the entire wafer surface; a total of 89 measurement locations for 300mm wafers and 21 locations for 200mm wafers. A MATLAB script was then used to fit a surface to the generated point cloud and extract the full 3-dimensional curvature of the wafer. Wafer warp was calculated in line with SEMI MF1390 [4], which for symmetrically warped wafers effectively translated to the maximum standoff height along the wafer periphery. A plot of the measurement locations and an example of extracted wafer curvature is shown in Fig. 1.

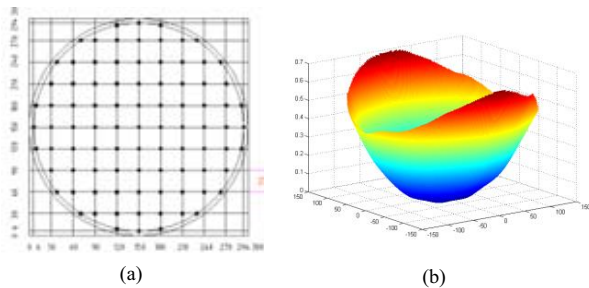


Fig. 1. (a) Coordinate locations for z-height measurement across a 300mm wafer, and (b) an example 3D surface fit to the measured point cloud.

C. Full Thickness Wafer Warpage Results

Measured warp for the full thickness wafer samples is shown in Fig. 2, where each point represents an average of at least four units. As expected, there is a general trend toward increased warp as the total metal film content increases. However, there is significant variation in the warp data within a given wafer size and film thickness. Additionally, we observed that the warpage shape varied from spheroidal to ellipsoidal and was characteristic to the layout design. As shown in Fig. 3, wafers with otherwise similar metal and polymer content had distinctly different warpage shapes and magnitudes, and were primarily differentiated by the design of the metal artwork itself.

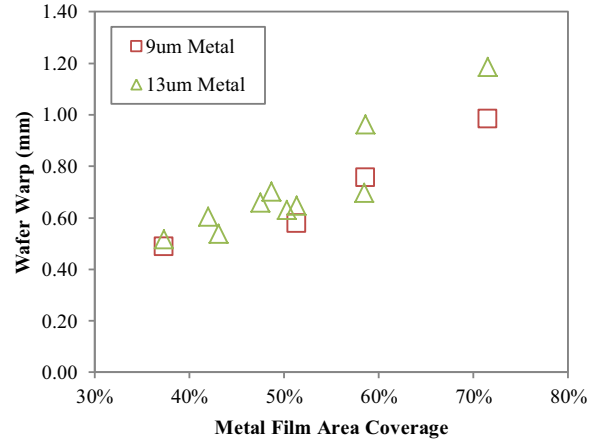


Fig. 2. Warp of full thickness 300 mm silicon wafers as a function of the metal pattern area coverage, for two different metal film thicknesses.

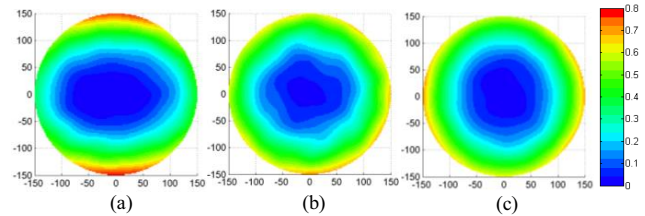


Fig. 3. Comparison of measured full thickness wafer warpage for three different layout designs with very similar metal film area coverage: (a) 48%, (b) 49%, and (c) 51%. Warpage shape ranges from spherical (b) to ellipsoidal (a, c). The same process, film thickness, and blanket polymer overcoat was applied to all three wafers, indicating that film layout geometry is responsible for the difference in warpage behavior.

D. Post-Backgrind Wafer Warpage Results

An additional set of 300 mm wafers was used to characterize the impact of wafer thinning on the warpage for five different pattern designs. Pre- and post-backgrind warp is shown in Fig. 4 for wafer thicknesses of 0.77, 0.25, and 0.17 mm. Overall the measured trends were observed to approximate the warp dependency on h_s^n . In fact it was empirically determined that on average $n \approx -2.0$ in alignment with (1) within the 0.17-0.25 mm silicon thickness range. However the warp increase due to thinning from 0.77 to 0.25 mm was systematically sharper, with $n \approx -2.3$. This data indicates that Stoney's formula can under-predict the post-backgrind warpage based on full thickness warp measurements, and should be used with caution.

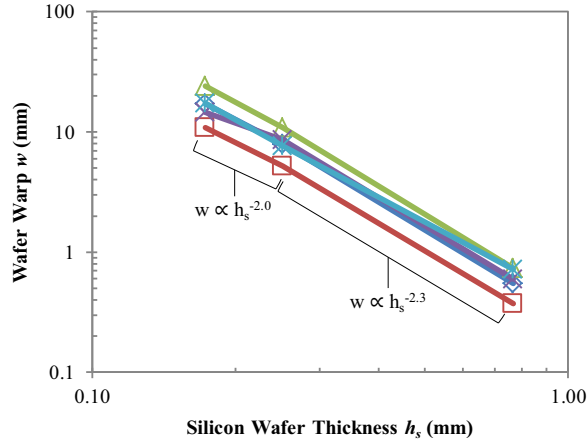


Fig. 4. Wafer warp as a function of silicon thickness for patterned 300 mm wafers. Each data series corresponds to a unique pattern layout.

The warpage shape was also observed to be strongly influenced by the wafer thickness, as shown in Fig. 5. At full thickness, all the measured samples showed a biaxial warpage shape, with curvature along major and minor axes that are orthogonal to the notch location. However upon backgrind to 0.25 mm and thinner, all the wafers collapsed into a predominantly cylindrical warpage shape. The transition from ellipsoidal to cylindrical warpage may also explain why the warp increased more rapidly than predicted by Stoney after backgrind to 0.25 mm thickness. This is likely due to nonlinear stiffening when wafers are biaxially warped, which acts to suppress the warp magnitude [3]. Thus the full thickness wafers warped less than Stoney’s prediction. However once the warpage converted to uniaxial curvature after backgrind, the warp followed closer to the predicted Stoney behavior with respect to wafer thickness, down to 0.17 mm for these evaluations.

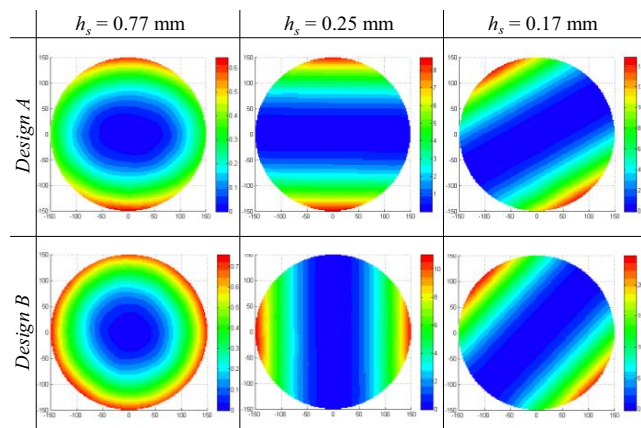


Fig. 5. Measured wafer warpage for two given layout patterns at three different silicon thicknesses, with notch facing down. Warpage shape changes from ellipsoidal to cylindrical, and increases in magnitude, as the wafer is thinned. When silicon wafer is thinned to 0.17 mm, the orientation of the major warp axis rotates off angle.

An interesting observation was that the major axis of curvature was typically maintained during the transition from

full thickness to 0.25 mm thickness. However after backgrind to 0.17 mm thickness, the major axis of curvature was rotated off-angle. The fact that the angle of this rotation was consistently measured as either ± 30 , ± 45 , or ± 60 degrees with respect to the notch location, seems to indicate that the silicon anisotropy and crystal orientation could be influencing the deformation at very high warp levels.

IV. MODELING

A. Modeling Methodology

A new modeling methodology was developed to capture the complex wafer warpage behavior observed in the characterized test vehicles, in order to accurately predict wafer warp for a given pattern, process technology, and backgrind thickness. As shown in Fig. 6, a two-level finite element approach was executed to predict the 3D wafer warpage for an arbitrary layout, as detailed in [2] and summarized here.

First a detailed 3D-solid die-level model including silicon substrate, top metal geometry, and polymer overcoat was used to simulate the film stress build up upon cooling down from high processing temperatures and thermal expansion mismatch between the various materials. The resulting film stress values, when averaged across the entire die, were then used as a basis to convert the multi-material, multi-layer, and multi-pattern film stack to an equivalent homogenized film. With a simple bilayer shell model representing just the effective film and silicon, the full 3D wafer warpage was then simulated under conditions mimicking the warpage measurement setup (i.e. laying active-side up on a flat table). Simulations were performed using ANSYS finite element software and automated using MATLAB scripting.

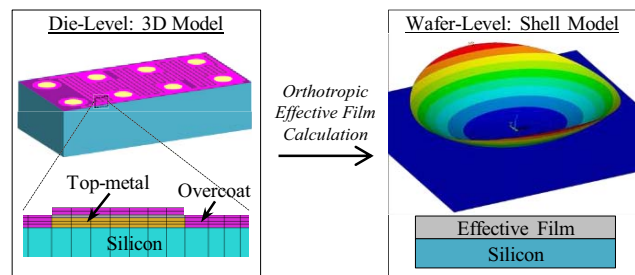


Fig. 6. Schematic illustration of the FEA model approach for wafer warp. A unit-cell die with patterned films is first modeled as a 3D-solid to capture the thermomechanical stress that accumulates within the complex film stack. The volume-averaged film stresses are then used to calculate an equivalent orthotropic film. Finally a bilayer shell model consisting of an effective homogeneous film and silicon substrate simulate the wafer warpage.

B. Die-Level Model

A single die unit-cell including silicon, patterned-metal, and patterned-overcoat was modeled using SOLID186 brick elements. All materials were defined as isotropic linear elastic, and Young’s modulus, Poisson’s ratio, and CTE was determined for each of the material components separately. In addition, an effective stress-free temperature, T_{refs} was initially defined for each of the film materials based on prior characterization of blanket film coated wafers. The resulting thermomechanical film stress was then simulated at room

temperature condition, and then volume averaged across the entire film stack to determine the total tension in the film as well as the principal stress orientations.

C. Homogenization of Thin Film Stack

The key to simplifying the model analysis for efficient warpage simulation was to reduce the geometric and material complexity of the patterned film stack on a die level to a homogenized effective film on a wafer level. Extraction of the effective film properties are based on averaged thermomechanical film stress resulting from CTE mismatch and thin film approximation described by

$$\alpha_{f,i}\Delta T + \varepsilon_{f,i} = \alpha_s\Delta T \text{ for } i = 1,2 \quad (3)$$

where α is the CTE, T is temperature, ε is mechanical strain, f and s correspond to effective film and silicon respectively, and subscript i corresponds to the orthogonal in-plane directions. In order for the effective homogenized film to capture the non-uniform stress that can result in ellipsoidal warpage modes, an orthotropic thin film constitutive model is used such that

$$\varepsilon_i = \frac{\sigma_i}{E_i} - \nu_j \frac{\nu_{ji}}{E_j} \text{ for } i, j = 1,2 \quad (4)$$

and the corresponding orthotropic symmetry constraint is

$$\frac{\nu_{ij}}{E_i} = \frac{\nu_{ji}}{E_j} \quad (5)$$

where σ is the film stress, E is the elastic modulus, and ν is Poisson's ratio. Substituting (4) into (3) and after some algebra results in

$$\frac{\sigma_i}{\Delta T} = m_i\alpha_s + b_i \text{ for } i = 1,2 \quad (6)$$

where the parameters m and b are used for brevity and are fully defined by the effective film mechanical properties as follows:

$$m_i = E_i \left(\frac{1 + \nu_{ji}}{1 - \nu_{ij}\nu_{ji}} \right) \quad (7)$$

$$b_i = -E_i \left(\frac{\alpha_i + \alpha_j\nu_{ji}}{1 - \nu_{ij}\nu_{ji}} \right) \quad (8)$$

It should be noted that (8) contains a minus sign in the beginning of the expression which was incorrectly omitted in [1].

Equation (6) demonstrates that for a given temperature differential, the thermomechanical film stress is a linear function of the substrate CTE. In other words, in order to solve for the two unknowns m and b , and by extension the effective

orthotropic film properties, we need to measure (or simulate) the film stress on at least two different substrates with different α_s . Thus, the die-level simulation could be executed twice – firstly using a conventional silicon substrate, and secondly using a substrate with an arbitrarily different CTE – and the resulting thermomechanical film stress for each case can be used to calculate an effective orthotropic film.

D. Wafer-Level Model

Once the effective film is calculated, it is used in a second wafer-level model to simulate the full 3D warpage using bilayer SHELL281 elements to represent the silicon and effective film. It should be noted that inclusion of non-linear geometry effects, gravity, and surface contact between the wafer and a flat rigid support (mimicking the measurement conditions) were all critically important to accurately predict the warpage. Non-convergence issues were overcome by activating both the contact elements and gravity in the first load step, and then applying the temperature differential in the following load step.

E. Model Results and Correlation

Simulations were first performed and correlated to the measured full thickness wafer warpage. Using the baseline film material properties initially defined for the metal and polymer films that are input into the die-level model, a reasonably accurate warpage prediction was able to be achieved. In order to further improve the accuracy of the simulations, the T_{ref} 's for each of the constituent material films was optimized to fit the data. In other words, the characteristic film stress for the metal and polymer films was adjusted until the warpage simulations aligned with the broad set of corresponding measurements. After a few iterations the film material properties were finalized, and the model was then correlated to the measured warpage within a tolerance of about ± 100 μm across the entire data set of full thickness wafer warpage as shown in Fig. 7. In addition to achieving a very good correlation to the wafer warp magnitude, the model also accurately captured the warpage shape, as an example comparison of model results and measured data is shown in Fig. 8.

After the model was optimized and correlated to the full thickness warpage data, the model was applied to thinned wafers to evaluate the prediction of post-backgrind warpage. Correlation of the simulation results to pre- and post-backgrind measurements is shown in Fig. 9. Again good agreement was achieved even for very high warp levels in the tens of millimeters for the thinnest wafers. Also important to note that the models correctly captured the cylindrical warpage shape after backgrind.

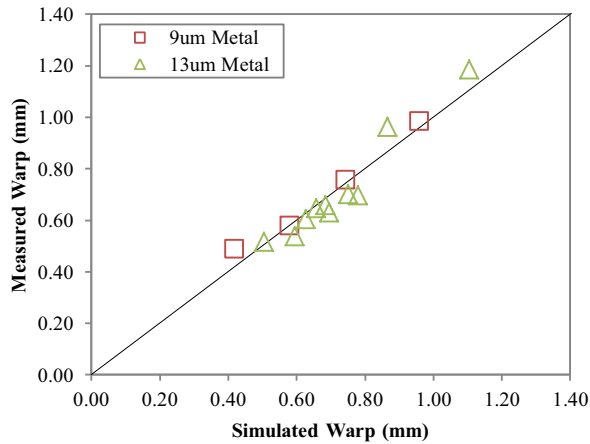


Fig. 7. Model correlation for full thickness wafer warpage across a spectrum of pattern designs, metallization thicknesses, and wafer diameter.

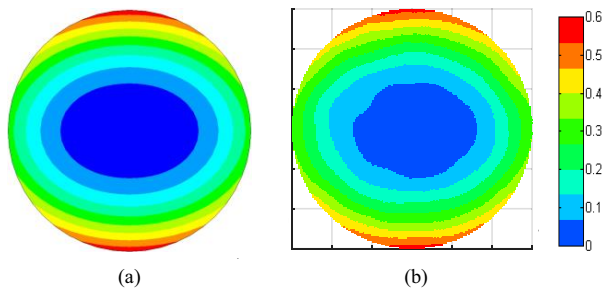


Fig. 8. Example correlation of full thickness wafer warpage magnitude and shape for a given pattern design between (a) FEA model and (b) empirical measurement.

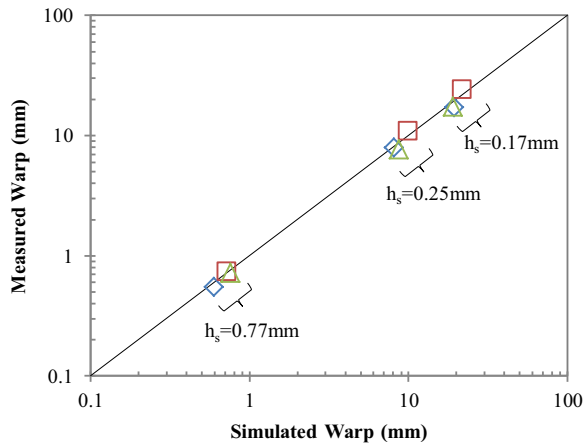


Fig. 9. Model correlation for 300 mm wafer warpage at three different wafer thicknesses. Each data series corresponds to a unique pattern design.

V. CONCLUSIONS

A study of wafer warpage behavior due to stress from patterned metal and polymer passivation films was performed. Test chip wafers were used to exercise metal design corners, and wafer warpage was characterized across a broad set of variables including metal film content, film thickness, artwork design, polymer overcoat pattern, and wafer thickness. Complex warpage shapes such as spherical, ellipsoidal, and cylindrical were observed, and the warpage magnitude and shape was characteristic to the different metal layouts evaluated. A key finding from this work is the design dependence of the top metal artwork on the warpage in addition to the metal content.

To understand the driving mechanisms and provide predictability to the warpage behavior, finite element models were developed which used the pattern designs and film material properties as inputs in order to simulate the resulting wafer warpage. A multi-scale modelling technique was developed that converts the composite film stack into an effective orthotropic film for efficient wafer-level warpage analysis. A robust modeling correlation to the measured warpage was achieved across the evaluated variables, and was able to capture both the warpage magnitude as well as the complex warpage shapes that arise from various layout geometries for both full thickness and post-backgrind wafers.

ACKNOWLEDGMENT

The authors would like to acknowledge Luis Rivera for his help with obtaining the wafers, and Noboru Nakanishi for the warpage measurements.

REFERENCES

- [1] G. Ostrowicki and S. Gurrum, "A stress-based effective film technique for wafer warpage prediction of arbitrarily patterned films," in ECTC, 2014 IEEE 64th, 2014.
- [2] G. G. Stoney, "The tension of metallic films deposited by electrolysis," *Proc. R. Soc. Lond. A*, vol. 82, no. 553, pp. 172-175, 1909.
- [3] L. Freund, J. Floro, E. Chason, "Extensions of the Stoney formula for substrate curvature to configurations with thin substrates or large deformations", *Appl. Phys. Lett.* 74, 1987 (1999).
- [4] SEMI MF1390-0707, "Test method for measuring warp on silicon wafers by automated non-contact scanning," San Jose, CA: SEMI, 2007.